DOI: 10.13009/EUCASS2022-7481

Interactions in micro-jets forced by dielectric barrier discharge

FRIDLENDER Tom[1], BENARD Nicolas*[2] and MOREAU Eric*[3]*

** Institut PPRIME - UPR 3346 – CNRS - Université de Poitiers - ISAE/ENSMA, SP2MI Téléport2 Bd Marie & Pierre Curie BP 30179, 86962 Futuroscope Chasseneuil Cedex, France*

[1]tom.fridlender@univ-poitiers.fr

[2]nicolas.benard@univ-poitiers.fr

[3]eric.moreau@univ-poitiers.fr

Abstract

An experimental investigation on control over micro-jet interactions with plasma dielectric barrier discharge (DBD) has been conducted. The authority of the DBD supplied with sinusoidal AC high voltage has been surveyed with low speed, high resolution particle image velocimetry (PIV). Two experiments are reported in this proceeding. First, the single micro-jet experiment sustains that the utilized electrode configuration is able to target the micro-jet preferred column mode. Then, micro-jet interactions that give rise to one lone macro-jet are investigated. It is observed that the less momentum imparting discharge at St_D=0.1 (210Hz), leads to the most drastic modification in terms of mean turbulent kinetic energy (TKE) distribution. It is suggested that the shear layer mode is involved with this unexpected result.

1. Introduction

Axisymmetric jets have attracted a lot of attention since the work of Crow and Champagne back in 1971 [1]. They observed that the jet preferred mode scaled with nozzle diameter and jet exit speed as $St_d=f\cdot d/U_{max}=0.3$ for different Reynolds numbers. They suggested that mixing is particularly enhanced by forcing the jet-column at a frequency that matches the preferred mode. Mattingly and Chang's linear spatial stability analysis [2], complementing Batchelor and Gill's work [3], shed light into Crow and Champagne's observations. They corroborated that initial conditions, i.e. the initial "top-hat" profile with an infinitely thin shear layer region, were of major importance. Most importantly, they stated that the near field column is unstable to all disturbances, particularly axisymmetric ones. Other experiments corroborated that the jet preferred mode was a global instability mechanism [4], [5]. It has even been observed downstream of multiple-jet systems [6], [7]. Multiple-jet interactions have been investigated most often on an array or on 2D jet clusters, where the small jets merge and give rise to a lone macro-jet [8], [9]. A few years ago, Benard et al., came up with the idea to control mixing downstream of a honeycomb micro-jet arrangement (121 micro-jets) by exciting the St_d=0.3 mode of the small jets with non-thermal plasma DBD [6], [7]. The plasma DBD is simply constituted with a dielectric plate separating one grounded electrode and an exposed conductor. The latter supplied by AC high voltage has extensively been used for the last 30 years as a flow control tool [10]. It features an active behavior, non-intrusive dimensions and fast response time capable of reattaching the flow along a NACA airfoil by its authority on coherent structures dynamics [11], inhibiting and catalyzing vortex pairing in a plane mixing layer [12]. In the above-mentioned experiments, the DBD's electromechanical conversion leading to a periodic jet flow has been availed to control instability mechanisms which is the key for scalability.

In Benard et al. investigations [6], [7], the DBD was able to enhance mixing downstream of the honeycomb jet arrangement. However, the most amplified mode scaled with the macro-jet diameter, a diameter 14 times larger than the micro-jets. Here, the honeycomb actuator has been modified to get 7 interacting micro-jets in the wake (one central jet and 6 surrounding ones). Macro to micro-jet diameter ratio is reduced to 3. This undergoing work motivations are diverse. First, it is meant to confirm that the DBD effectively targets the micro-jet preferred mode. Then it is expected to get better understanding on micro-jet interactions and how to actively assist them, which is of major importance to diminish heat dispersion, unburnt fuels and noise reduction in many applications related to aeronautics.

DOI: 10.13009/EUCASS2022-7481

2. Experimental apparatus and procedure

The utilized actuator is a 1.3mm thin perforated multi-layer ceramic plate equipped with a plasma DBD system. A conductive Nickel layer with minimal protrusion of 10µm serves as an active electrode where high voltage is applied. The voltage is a sinusoidal wave of E_{AC} amplitude and f_{AC} frequency supplied by a TREK model 20/20C-HS high voltage amplifier. A counter electrode connected to the ground is embedded in the ceramic material. The holes are 7 circles with a 2mm diameter distributed as displayed in Figure 1(a). As mentioned in the introduction, this actuator is similar to the one used by Benard et al. Indeed, the exposed electrode has been modified such that only the 7 central holes will be subjected to a periodic jet flow resulting from electromechanical conversion of the DBD. The remaining jets are blocked from both sides of the plate with Kapton adhesive tape.

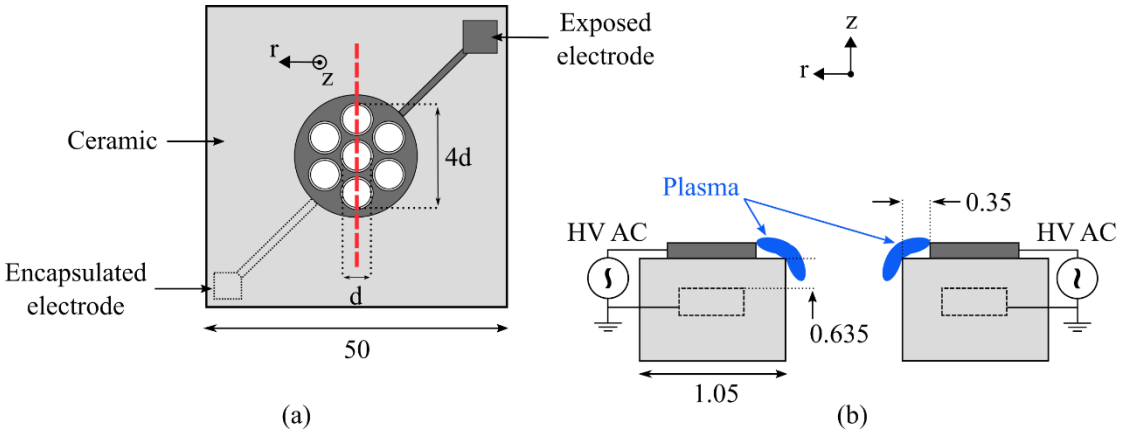

Figure 1: Multi-jet actuator front schematic with laser sheet impact represented by the dashed red line (a) and cross plane displaying electrode placement around one hole with plasma ignition in blue [not to scale, dimensions in mm]

Experiments are conducted in a circular open blowing wind-tunnel ended by a jet exit of 50 mm inner diameter. The perforated ceramic plate is maintained at the exhaust of the wind-tunnel with a special inhouse designed PMMA piece. The latter is positioned such that the embedded electrode is the closest to the exhaust. Plasma ignites from all across the inner electrode's edge and finds its way inside each circular hole. In the plasma region, the electric field periodically surpasses the breakdown value at which the surrounding air is ionized. That same electric field guides ions and charged particles transfer momentum to neutral ones by colliding with them. Momentum transfer results in a jet flow originating at the inner edge of the exposed electrode at a mean speed of u_r=-0.4m/s when E_{AC}=5kV and f_{AC}=2kHz. The jet goes around the holes edges and is directed towards the embedded electrode at a core mean speed of u_z=-1m/s with the same discharge conditions according to Benard et al. [6]. Moreover, for a given voltage amplitude E_{AC}, power consumption and input momentum increase with f_{AC} frequency. So, in both experiments described in this article, increasing the frequency also means increasing input momentum. However, the jet velocity is not constant in time. The electric field's alternative nature results in the so called "push-push" dynamic of the forcing, meaning that the DBD is pushing nearby air at the same frequency than the voltage supplied to the exposed electrode.

The wind tunnel fan is set to get a micro-jet exit speed of 15.6m.s^{-1} (Re_d=2·10^3) for the single jet characterization as well as for the interacting jets experiment. A low speed, high-resolution PIV system is used to measure the time-averaged flow field in the wake of the perforated plate. The field is 60 mm in the z direction by 40 mm in the r direction and starts 1 mm downstream of the plate because of laser reflections. The flow is seeded with Ondina 15 particles of an average size of 0.5µm thank to an ATM 220 aerosol generator. Particles reflect the light from a laser sheet obtained with two aligned Nd-YAG Big Sky Laser beams shot through an optical arrangement. Their wavelength is 532nm and pulse energy is 250mJ over 9nsec. The optical arrangement is composed of a concave lens followed by a convex and a cylindrical one. It is set to give a 1mm thin laser sheet hitting the plate as the dashed red line on Figure 1(a). Each laser is shot at 4.4Hz with an adjustable delay between them to control maximum particle displacement (Δt=7µs). Snapshots are captured with a LaVision Imager LX. The CCD sensor has a resolution of 16 MP and encodes grayscales with a 12 Bit depth. The camera is equipped with a 100mm LAOWA Dreamer Macro 2X lens (Ø67mm). F-stop is set at 5.6 during all experiments.

Mean, standard deviation velocity fields and other turbulent quantities (i.e. Reynolds stresses components and Turbulent Kinetic Energy) are calculated with Davis 10.2. Calculations are made on 3 000 instantaneous fields for the baseline flow and both the St_d=0.3 and St_D=0.3 controlled cases. 1 500 instantaneous fields are used for the remaining cases. The discharge is turned on for 5 to 10 seconds before starting every PIV run.

For the single micro-jet experiment, vectors are calculated with the following multi-pass algorithm: one pass with a 64·64 window size (50% overlap) followed by two passes with a 24·24 window size (50% overlap) using a weighing

DOI: 10.13009/EUCASS2022-7481

function. Vectors are deleted and replaced by interpolation if peak to noise ratio is over 1.7. A median filter is also applied between passes. It results in 1 vector being computed every 153µm. For the multiple micro-jets experiment and the single micro-jet initial profile description, vectors are calculated with the following multi-pass algorithm: one pass with a 64·64 window size (50% overlap) followed by two passes with a 16·16 window size (50% overlap) using a weighing function. Vectors are deleted and replaced by interpolation if peak to noise ratio is over 1.55. A median filter is also applied between passes. It results in 1 vector being computed every 102µm.

3. Single micro-jet characterization and control

For the first experiment, peripheral jets are blocked with a Kapton adhesive tape on both sides of the plate. In the aforementioned configuration, the single jet flow is achieved and the 6 peripheral discharges cannot interfere with the flow development. Nonetheless, the central hole's DBD generates a velocity fluctuation that "pinches" the micro-jet column at the hole's exit at f_{AC} frequency. Therefore, this experiment serves to investigate the behavior of the single jet given its small d=2mm diameter and the 25:1 abrupt contraction condition upstream. Moreover, it is necessary to investigate this DBD's authority over a single micro-jet.

3.1. Baseline flow description

The initial profile is extracted from the mean velocity field at z/d=1 (see Figure 3). It is in good agreement with Namer and Ötügen's plane jet profile extracted at z/d=1 with a nozzle width of d=3mm and $Re_d=2\cdot10^3$ [13]. Grandchamp and Van Hirtum [14] also observed a similar profile at z/d=0.04 on their round air jet downstream of an abrupt 40:1 contraption with a nozzle length to diameter ratio of L/d=1.2 (0.65 in the present case) at $Re_d=2.3\cdot10^3$. The hyperbolic tangent formula (1) taken from [15] fits the half-profile with a 2.7% root mean square error (RMSE). A Levenberg-Marquardt algorithm with a nonlinear least square method is used.

$$\frac{u_z(r)}{U_c} = \frac{1}{2}\left(1 + \tanh\left(\frac{r_0 - r}{2\delta_{\theta 0}}\right)\right) \quad \textbf{(1)}$$

The considered momentum thickness is calculated with equation (2) where U_c is the centerline mean axial velocity. The profile clearly has a "top-hat" shape. Momentum thickness over nozzle diameter ratio is $\delta_{\theta 0}/d=3\cdot10^{-2}$. The thin shear layer hypothesis can be considered as valid and, according to Mattingly and Chang's theoretical work [2], both of these conditions indicate that this jet flow is unstable to all disturbances and particularly axisymmetric ones in the near field.

$$\delta_\theta = \int_0^\infty \frac{u_z}{U_c}\left(1 - \frac{u_z}{U_c}\right) dr \quad \textbf{(2)}$$

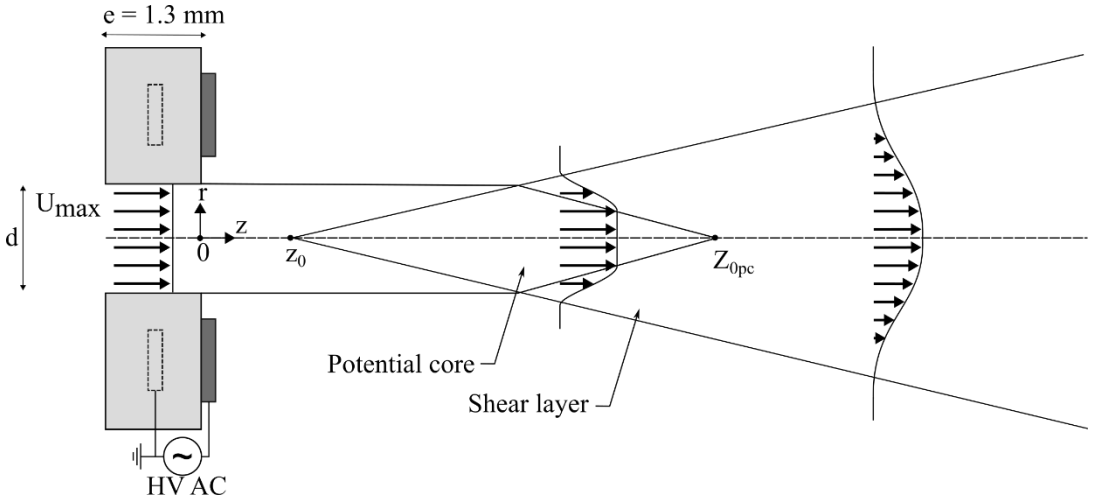

Figure 2: Central jet mean flow field scheme in the PIV plane

DOI: 10.13009/EUCASS2022-7481

The mean axial velocity decay along the centerline is in good agreement with Nammer and Ötügen's previously cited results and with Hrycak et al. work [16] on a round air jet impinging on a flat plate. In the latter investigation, nozzle diameter was d=3.2mm, $Re_d=2.1\cdot10^3$ and the jet behavior is proven similar to a free jet within the region where data has been extracted. Regarding Grandchamp and Van Hirtum experiments, they measured an abrupt decay between the nozzle exit and the z/d=1 station. We are not able to compare our data to their results due to laser reflections. Nonetheless, they obtained a much shorter potential core length of 4d, unlike the present results that agree with a baseline potential core length of 8.7d obtained by other experimenters on typical round jets at $Re_d=2\cdot10^3$ [17].

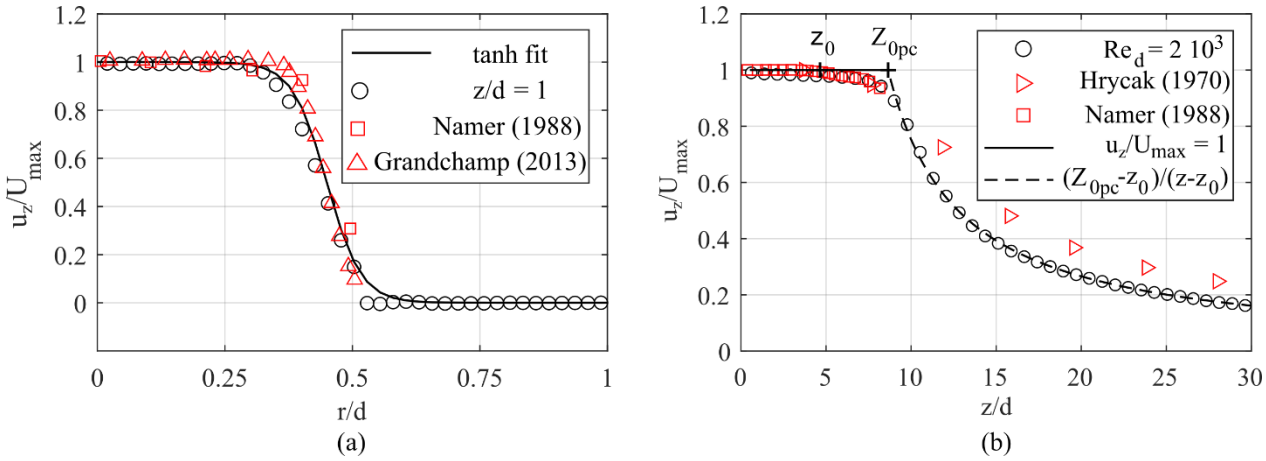

Figure 3: Initial profile extracted at z/d=1 (a) and mean axial velocity decay along the centerline (b) for the single micro-jet

Figure 3(b) concurs with the idea that the mean field can be split into three zones, each broadly described in jet experiments. The near field is essentially a laminar air column moving on average at $u_z/U_{max}=1$ surrounded by stagnant air. Then, the virtual origin located at z_0/d=4.7 marks the average position after which coherent structures start appearing and entraining ambient fluid into the jet [18] thereby progressively reducing the potential core average cross section. As a consequence, the mean axial velocity slowly decays until the potential core ends at Z_{0pc}/d=8.7. From then on, in the zone of established flow, axial velocity decays as $u_z/U_{max}=(Z_{0pc}- z_0)/(z- z_0)$ [19] with a 0.9% RMSE. The second equation is fitted to the mean axial velocity from the shear layers intersection point, given by a peak in TKE, until the end of the domain. Z_{0pc} is then defined as the intersection between the $u_z/U_{max}=1$ and the $u_z/U_{max}=(Z_{0pc}- z_0)/(z- z_0)$ curves.

3.2. Single micro-jet preferred mode excitation

One typical manner to measure the influence of a flow control device is to determine the location where the potential core ends for different input disturbances. However, care must be taken when comparing potential core lengths. Or et al. [20] reviewed this problem with round jets in co and counter flowing environments where the virtual origin can be located slightly upstream of the jet exit or as much as 5 nozzle diameters downstream. Figure 4(a) shows that the virtual origin z_0 is shifted close to the jet exit when the discharge is turned on. It goes from -0.2d to 0.4d depending on the AC frequency at E_{AC}=5kV. This indicates that the ionic wind effectively inputs velocity at the jet exit. Additional mean axial velocity decay curves (not shown in the present document) feature slow decay rates from the first measurement location until the end of the potential core.

DOI: 10.13009/EUCASS2022-7481

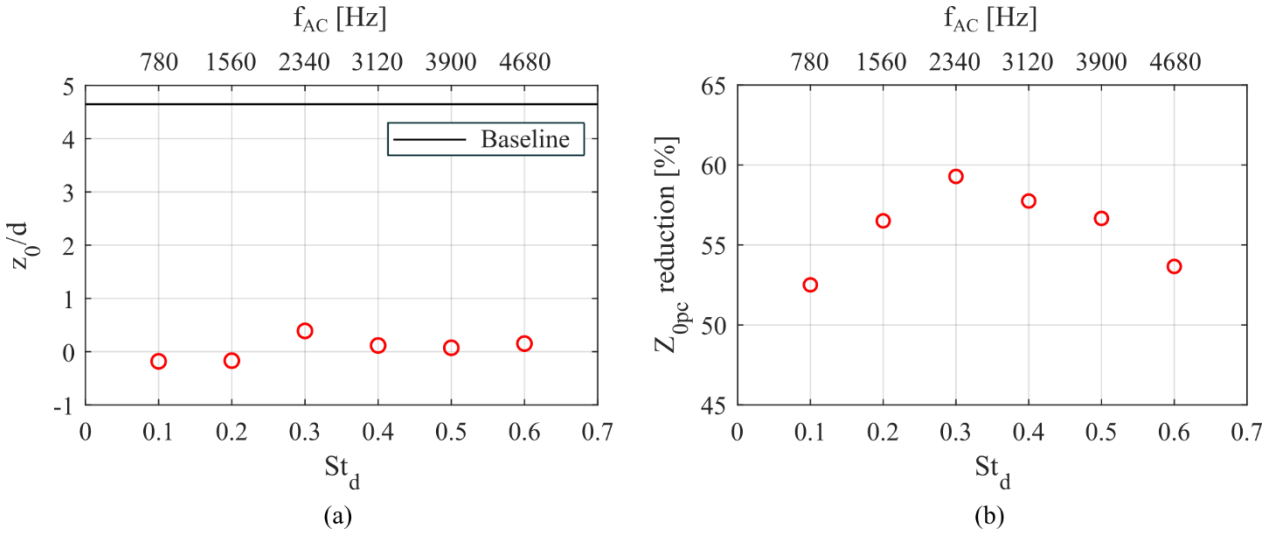

Figure 4: Virtual origin (a) and potential core length (b) of the single central jet versus St_d excitation on the bottom axis (frequency equivalence on the top axis)

Figure 4(b) displays the shortest potential core length for an excitation at St_d=0.3 (f_{AC}=2 340Hz) and E_{AC}=5kV. Nonetheless, 48% of the potential core reduction is due to the virtual origin shifting from z_0=4.7d to z_0=0.4d. Effective reduction is considered to be 12% at St_d=0.3. It is worth noting that U_{max} varies within ±1% of the baseline jet exit speed when the discharge is active. This indicates that the discharge does not input too much momentum in the jet flow, thereby, it doesn't seem to overrule the instability mechanism. Further and finer results are being analyzed for a better estimation of the mean momentum imparted in the shear layer. However, the St_d=0.3 mode is indeed the most amplified among the 6 tested ones.

4. Interacting micro-jets characterization and control

4.1. Baseline flow description

The dielectric Kapton tape is removed to release the 6 peripheral jets and the fan is adjusted to get a central micro-jet exit speed of U_{max}=15.6m.s^{-1}. Particle snapshots, as Figure 5(a), clearly feature coherent structures developing in the shear layers while each jet is still distinguishable. Then, one macro-jet seems to arise from amalgamation of the micro-jets. The mean field on figure 5(b) reveals that indeed the top and bottom jets are entrained towards the center. All jets eventually coalesce and one lone self-similar mean profile is observed.

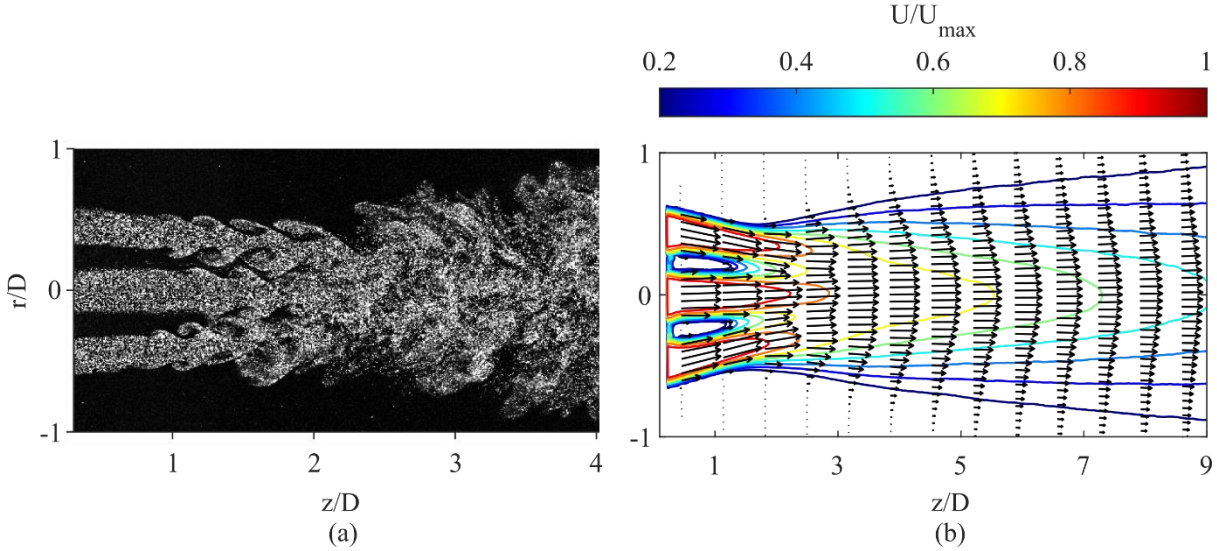

Figure 5: Particle snapshot zoomed view (a) and mean field with velocity magnitude contours (b)

DOI: 10.13009/EUCASS2022-7481

The initial micro-jet profiles extracted at z/d=1 are displayed in figure 6(a). All three have top-hat profiles, see Figure 6(a), but the top and bottom micro-jets converge towards the center respectively at mean radial velocities of - $0.05 \cdot U_{max}$ and $0.06 \cdot U_{max}$. Farther downstream, one can find the first location where the term du_z/dr changes from positive to negative only at r/D=0 (see Figure 6(b)). The latter, noted as Z_x=3.3, is considered as the physical origin of the macro-jet. Equation (1) fits the main jet half-profile with a 7.4% RMSE. The profile is neither a "top-hat" nor a fully developed profile. The r_0 value is extracted from Figure 6(b). Here, the macro-jet diameter is determined with the $U_x/2$ criterion giving r_0=D/2 with D=6mm. Initial top shear layer momentum thickness $\delta_{\theta 1}/D=9 \cdot 10^{-2}$ is calculated from equation (2) with a centerline velocity of $U_c=U_x$ (U_x=12m.s^{-1}, $Re_D=4.6 \cdot 10^3$).

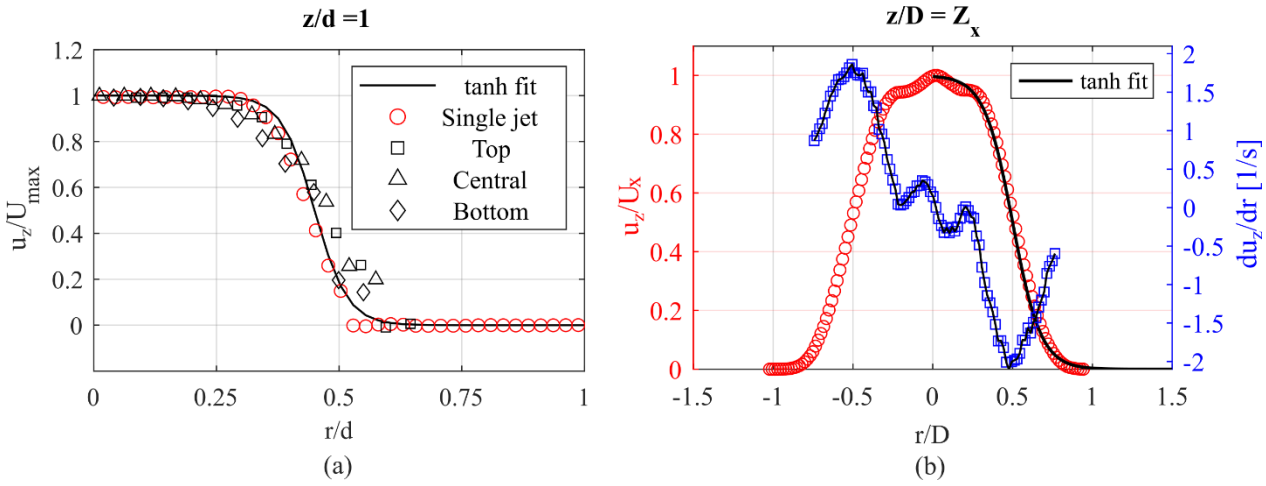

Figure 6: Initial profile of the top, central and bottom micro-jets compared to the single micro-jet case (a) and macro-jet profile at its physical origin Z_x (b) with hyperbolic tangent fit

The mean axial velocity decay along the centerline is represented in Figure 7(a). The central micro-jet exits the hole at u_z/U_{max}=1. The first velocity drop is observed from the location where both central shear layers start developing (around z/D=1.2) and ends right after the first TKE peak (see Figure 7(a) and (b)). Then, from the macro-jet physical origin Z_x, a slow and monotonous decay settles in the main potential core. Finally, past Z_{1pc}, mean axial velocity decays as for a single jet and TKE energy peaks for the second time farther downstream.

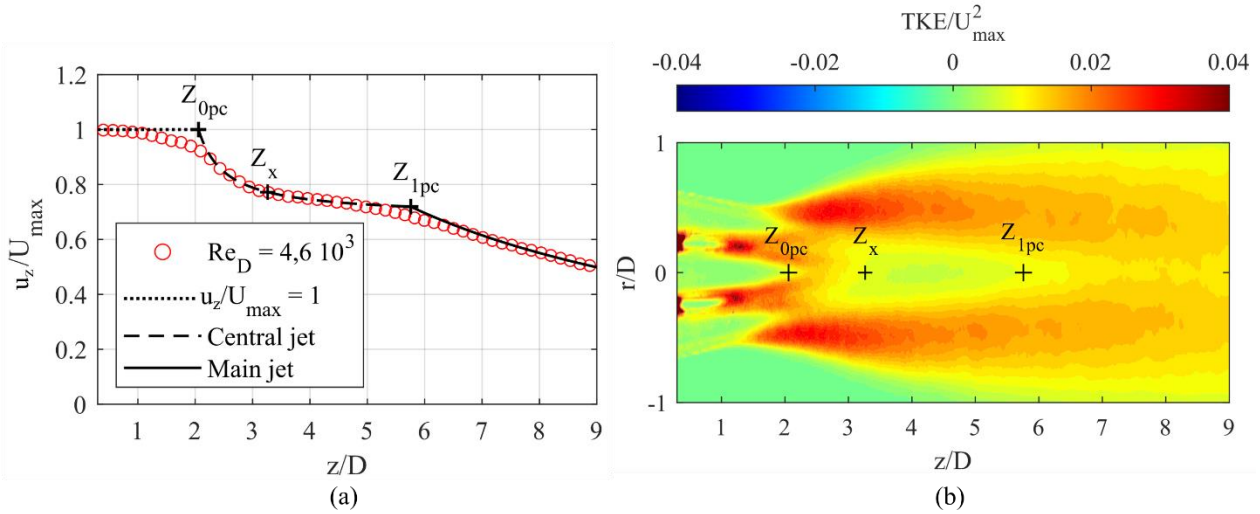

Figure 7: Mean axial velocity decay along the centerline with fitted functions (a) and TKE field (b) both with Z_{0pc}, Z_x and Z_{1pc} locations

Model equations (3) and (4) can be used to determine both the Z_{0pc} and the Z_{1pc} locations. The latter respectively fit the data with a 0.27% RMSE and a 0.24% RMSE.

$$\frac{u_z}{U_{max}} = \frac{a - z_0}{z - z_0} + b \qquad \textbf{(3)}$$

DOI: 10.13009/EUCASS2022-7481

$$\frac{u_z}{U_{max}} = \frac{c - z_1}{z - z_1} \quad \textbf{(4)}$$

Both the Z_{0pc} and the Z_{1pc} locations are determined by solving the intersecting points respectively given by $(a- z_0)/(Z_{0pc}- z_0)+b=1$ and $(a- z_0)/(Z_{1pc}- z_0)+b=(c- z_1)/(Z_{1pc}- z_1)$. The latter are in good agreement with mean TKE contours featured in Figure 7(b) provided that there are enough data points to fit equation (4) and that there is a macro-jet potential core. As a consequence, only the profile analysis and equation (3) will be used in the next section to determine both Z_x and Z_{0pc} locations.

4.2. DBD's authority over jet interactions

Results in section 2 indicate that the DBD inputs momentum at the grid exit and minimizes the single central micro-jet potential core length at St_d=0.3 (f_{AC}=2 340Hz). Moreover, Benard et al. [6], [7] used a similar grid where a whole 121 jet honeycomb pattern was active. In their experiment, they showed that the most amplified wave in the wake scaled with the macro-jet diameter as St_D=0.32. In this section the DBD authority over micro-jet interactions is discussed. Voltage amplitude is kept at E_{AC}=6kV and AC frequency is firstly changed from 210Hz to 1 260Hz with a 210Hz step to target the macro-jet modes going from St_D=0.1 to 0.6 (with a step of 0.1). Then, AC frequency is changed from 780Hz to 4 680Hz with a 780Hz step to target the micro-jet modes in the same way.

The first thing that stands out is that the discharge effectively acts on the near field for all tested AC frequencies. According to Figure 8(a), (b) and (c), the first TKE peak location along the centerline correlates to the micro-jet potential core length whatever the AC frequency among tested values. It also correlates to the macro-jet physical origin on Figure 8(d). Linear fits respectively give a growth rate of 1.3 with a 5.4% RMSE on Figure 8(c) and a growth rate of 0.72 with a 11.6% RMSE on Figure 8(d). Both correlations corroborate that the fitting method and the profile analysis can be used to determine respectively Z_x and Z_{0pc}. They most importantly show that the more the AC frequency increases, the more it acts on micro-jets with an optimal excitation at St_d=0.4.

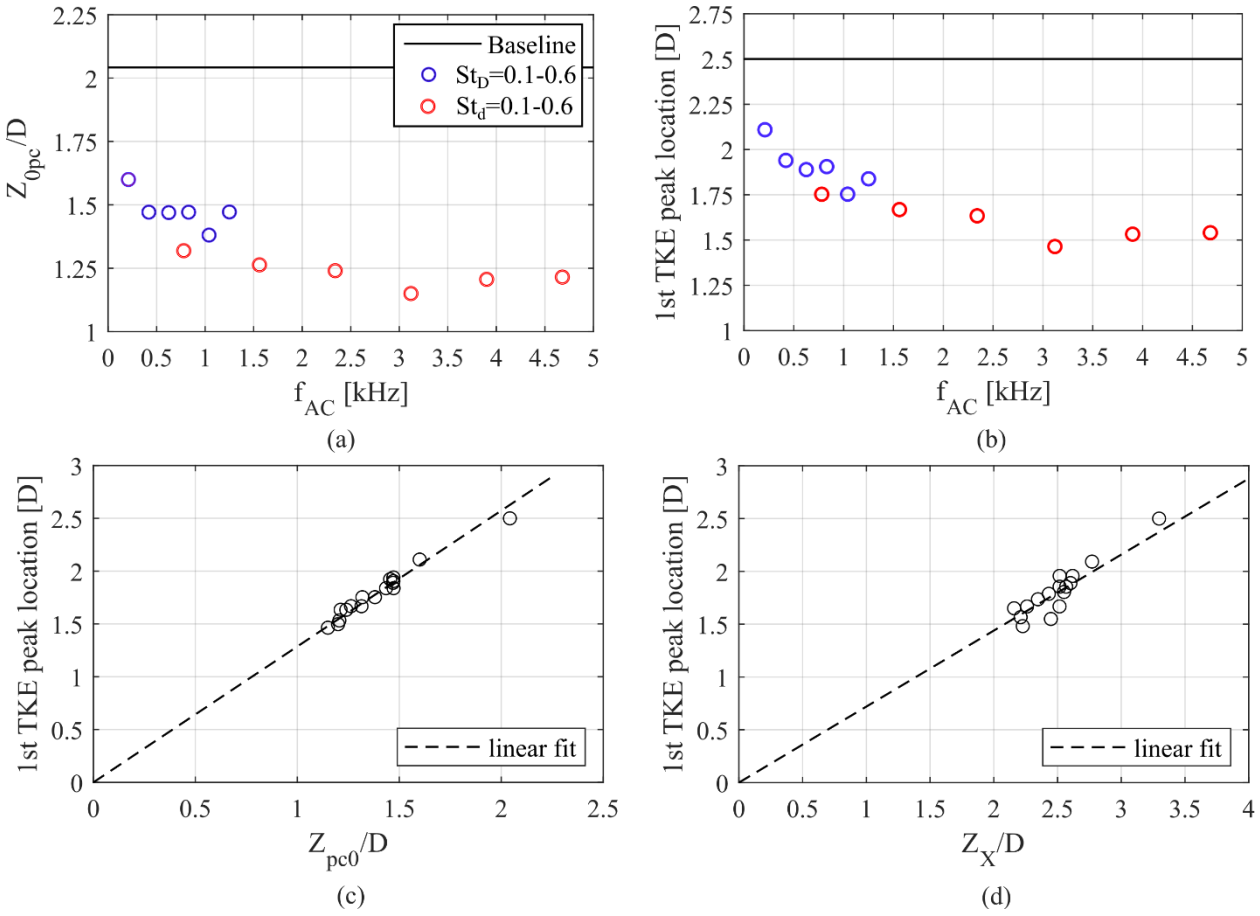

Figure 8: Central micro-jet potential core length (a), first TKE peak location along the centerline (b) plotted against f_{AC} at E_{AC}=6kV (macro-column modes in blue, micro-column modes in red). First TKE peak location along the centerline versus central-micro-jet potential core length (c) and macro-jet physical origin (d) all cases considered

DOI: 10.13009/EUCASS2022-7481

Indeed, the minimal micro-core length is achieved for St_d=0.4 (f_{AC}=3 120Hz). The St_d=0.4 excitation also leads to the earliest and highest mean TKE peak along the centerline (see Figure 9(b)). Additionally, it leads to the most important mean axial velocity decay within the domain. As consequence, one can postulate that it is the central micro-jets preferred mode in this flow configuration. Nonetheless, its influence on macro-jet potential core length does not stand out on Figure 10(d).

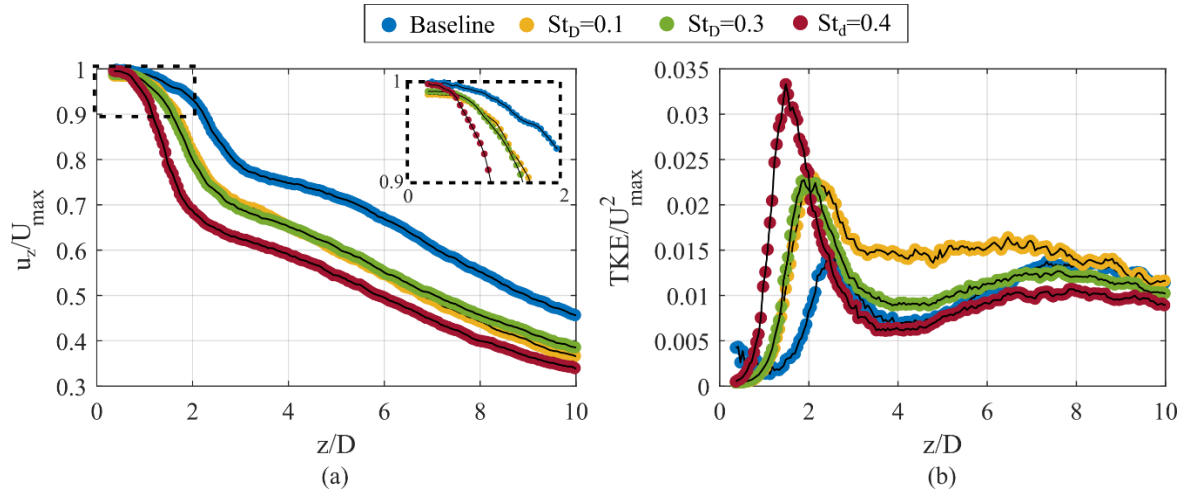

Figure 9: Centerline extraction of mean axial velocity with zoomed nearfield view on the top right (a) and mean turbulent kinetic energy (b) for the baseline flow and the forced flow at E_{AC}=6kV and St_D=0.1, St_D=0.3, St_d=0.4

From mean TKE contours on figure 10, one can see that the St_D=0.3 excitation has indeed more influence than the St_d=0.4 in terms of macro-jet potential core length. However, the St_D=0.1 case is unexpectedly the one leading to the most drastic change in terms of mean TKE distribution, i.e. mixing within the plane of measurement. No macro-jet potential core is visible neither on Figure 10(b) nor on Figure 9(b) where one lone TKE peak is observed along the centerline. This case arouses interest for three main reasons. Firstly, it is the least momentum imparting and power consuming discharge here tested. Secondly it is not clear whether or not velocity decay curves intersect for St_d=0.4 and St_D=0.1 downstream of z/D=10. Thirdly, it scales with shear layer momentum thickness at z/D=Z_x as $St_{\delta\theta}=(f_{AC}\cdot\delta_{\theta 1})/U_x=0.095$. This value is close to the $St_{\delta\theta}$=0.012 value reported in the literature as the shear layer mode.

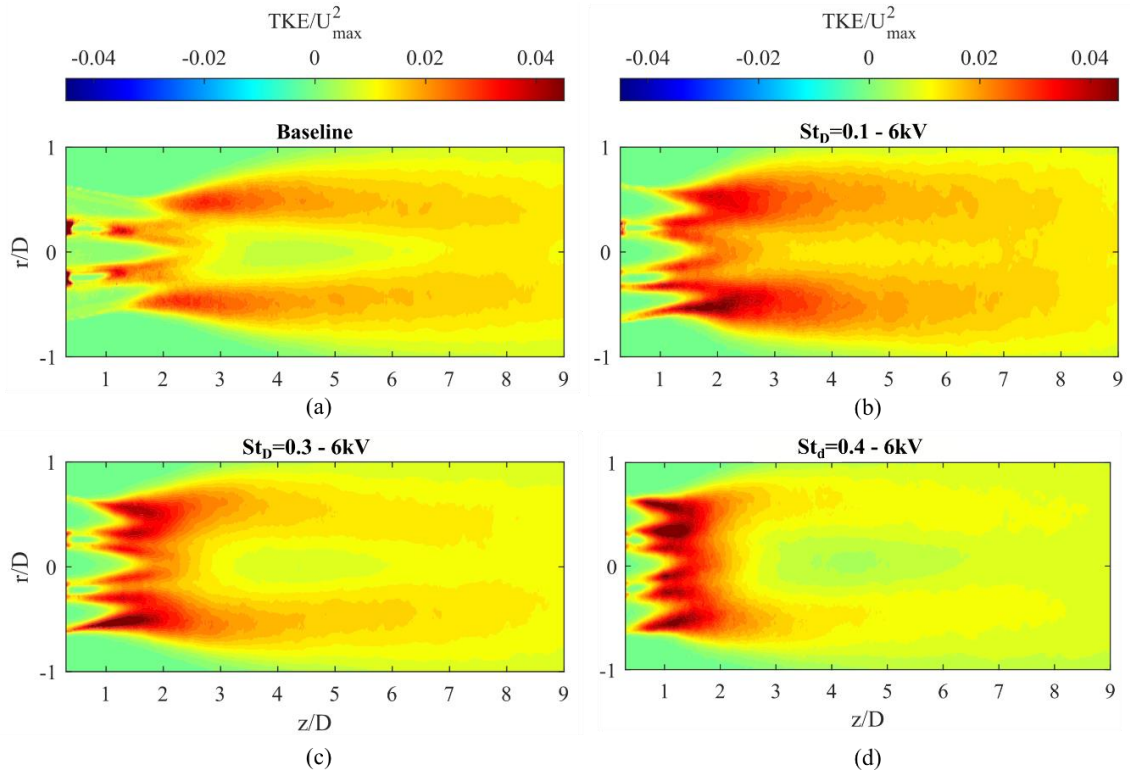

Figure 10: TKE field for the baseline flow (a), the forced flow at EAC=6kV and St_D=0.1 (b), St_D=0.31 (c) St_d=0.4 (d)

5. Concluding remarks

An experimental investigation on control over micro-jet interactions has been carried. The plasma DBD's authority has been surveyed with low speed, high resolution particle image velocimetry (PIV). The DBD was supplied by AC high voltage for two experiments.

In the first experiment, the DBD was used to target the preferred mode of a micro-jet behaving like a typical subsonic round jet at $Re_d=2\cdot10^3$. One AC frequency sweep corresponding to Strouhal numbers (based on micro-jet diameter) going from 0.1 to 0.6 with a 0.1 step reveals that the potential core length is minimized when the discharge frequency is set to excite the $St_d=0.3$ mode. A potential core reduction of 58% is achieved with a relatively low 5kV amplitude and no burst modulation applied. Moreover, the micro-jet virtual origin shifts from 5 nozzle diameters downstream of the jet exit to the jet exit where the exposed electrode is located. The discharge seems to input momentum fluctuations at the micro-jet exit, thereby allowing it to target the micro-column instability. Complementary data on lower frequencies, burst modulation and higher voltage amplitude discharges is being processed and is expected to feature augmented DBD authority over the jet, particularly at the $St_d=0.3$ value. Time resolved PIV or Laser Doppler Velocimetry will be utilized in the near future to characterize the velocity fluctuations imparted by the discharge.

The second experiment involves 7 interacting micro-jets. They are shown to amalgamate and give rise to a single macro-jet in their wake. The PIV center plane clearly reveals the micro-jets and the macro jet potential cores. The DBD is used to target the small and the macro-column modes as in the first experiment. The fastest mean axial velocity decay within the domain is obtained with a excitation at $St_d=0.4$ excitation. However, the most drastic change in terms of mean TKE distribution is observed at the lowest frequency (i.e., the less momentum imparting and power consuming discharge tested). That frequency scales with initial shear layer momentum thickness as $St_{\delta\theta}=0.095$. It is suggested that maximum mixing enhancement could be achieved through shear layer mode excitation in this configuration. Complementary data on burst modulation discharges is expected to corroborate these results. Also, future experiments on shear layer mode excitation will be conducted to gain better understanding of the instability mechanism reported in this article.

Acknowledgment

A part of the experimental equipment used in this work was funded by the French Government program Investissements d'Avenir (LABEX INTERACTIFS, reference ANR-11-LABX-0017-01).

References

[1] S. C. Crow and F. H. Champagne, "Orderly structure in jet turbulence," *J. Fluid Mech.*, vol. 48, no. 3, pp. 547–591, Aug. 1971.

[2] G. E. Mattingly and C. C. Chang, "Unstable waves on an axisymmetric jet column," *J. Fluid Mech.*, vol. 65, no. 3, pp. 541–560, Sep. 1974.

[3] G. K. Batchelor and A. E. Gill, "Analysis of the stability of axisymmetric jets," *J. Fluid Mech.*, vol. 14, no. 04, p. 529, Dec. 1962.

[4] A. K. M. F. Hussain and K. B. M. Q. Zaman, "The 'preferred mode' of the axisymmetric jet," *J. Fluid Mech.*, vol. 110, pp. 39–71, Sep. 1981.

[5] M. Samimy, J.-H. Kim, J. Kastner, I. Adamovich, and Y. Utkin, "Active control of high-speed and high-Reynolds-number jets using plasma actuators," *J. Fluid Mech.*, vol. 578, pp. 305–330, May 2007.

[6] N. Benard, A. Mizuno, and E. Moreau, "Active Multiple Jets System Using Surface Plasma Actuator," presented at the 8th AIAA Flow Control Conference, Washington, D.C., Jun. 2016.

[7] N. Benard, P. Audier, E. Moreau, K. Takashima, and A. Mizuno, "Active plasma grid for on-demand airflow mixing increase," *J. Electrost.*, vol. 88, pp. 15–23, Aug. 2017.

[8] M. Boutazakhti, P. E. Sullivan, M. J. Thomson, and I. Yimer, "Flow Downstream of a Cluster of Nine Jets," *J. Fluids Eng.*, vol. 129, no. 5, pp. 541–550, May 2007.

[9] S. Ghahremanian, K. Svensson, M. J. Tummers, and B. Moshfegh, "Near-field development of a row of round jets at low Reynolds numbers," *Exp. Fluids*, vol. 55, no. 8, p. 1789, Aug. 2014.

[10] N. Benard and E. Moreau, "Electrical and mechanical characteristics of surface AC dielectric barrier discharge plasma actuators applied to airflow control," *Exp. Fluids*, vol. 55, no. 11, p. 1846, Nov. 2014.

[11] N. Benard and E. Moreau, "On the Vortex Dynamic of Airflow Reattachment Forced by a Single Non-thermal Plasma Discharge Actuator," *Flow Turbul. Combust.*, vol. 87, no. 1, pp. 1–31, Jul. 2011.

[12] S. Yadala Venkata, N. Benard, M. Kotsonis, and E. Moreau, "Effect of DBD plasma actuation on structures in a plane mixing layer," presented at the AIAA Scitech 2020 Forum, Orlando, FL, Jan. 2020.

DOI: 10.13009/EUCASS2022-7481

[13] I. Namer and M. V. Ötügen, "Velocity measurements in a plane turbulent air jet at moderate Reynolds numbers," *Exp. Fluids*, vol. 6, no. 6, pp. 387–399, Jan. 1988.
[14] X. Grandchamp and A. Van Hirtum, "Near Field Round Jet Flow Downstream from an Abrupt Contraction Nozzle with Tube Extension," *Flow Turbul. Combust.*, vol. 90, no. 1, pp. 95–119, Jan. 2013.
[15] C. Bailly and G. Comte-Bellot, *Turbulence*. Cham: Springer International Publishing, 2015.
[16] P. Hrycak, D. T. Lee, J. W. Gauntner, and J. N. B. Livingood, "Experimental flow characteristics of a single turbulent jet impinging on a flat plate," NASA, Springfield, Virginia 22151, Technical Note NASA TN D-5690, 1970.
[17] T. L. Labus and E. P. Symons, "Experimental investigation of an axisymmetric free jet with an initially uniform velocity profile," NASA, Cleveland, Ohio 44135, Technical Note NASA TN D-6783, 1972.
[18] D. Liepmann and M. Gharib, "The role of streamwise vorticity in the near-field entrainment of round jets," *J. Fluid Mech.*, vol. 245, no. 1, p. 643, Dec. 1992.
[19] Y. Antoine, F. Lemoine, and M. Lebouché, "Turbulent transport of a passive scalar in a round jet discharging into a co-flowing stream," *Eur. J. Mech. - BFluids*, vol. 20, no. 2, pp. 275–301, Mar. 2001.
[20] C. M. Or, K. M. Lam, and P. Liu, "Potential core lengths of round jets in stagnant and moving environments," *J. Hydro-Environ. Res.*, vol. 5, no. 2, pp. 81–91, Jun. 2011.